

**Higher order coherence of exciton-polariton condensates**Tomoyuki Horikiri,<sup>1,2</sup> Paolo Schwendimann,<sup>3</sup> Antonio Quattropani,<sup>3</sup> Sven Höfling,<sup>4</sup> Alfred Forchel,<sup>4</sup> and Yoshihisa Yamamoto<sup>1,2</sup><sup>1</sup>*National Institute of Informatics, Hitotsubashi, Chiyoda-ku, Tokyo 101-8430, Japan*<sup>2</sup>*E. L. Ginzton Laboratory, Stanford University, Stanford, California 94305-4088, USA*<sup>3</sup>*Institute of Theoretical Physics, École Polytechnique Fédérale de Lausanne (EPFL), CH 1015 Lausanne, Switzerland*<sup>4</sup>*Technische Physik, Universität Würzburg, Am Hubland, D-97074 Würzburg, Germany*

(Received 30 November 2009; revised manuscript received 16 December 2009; published 25 January 2010)

The second- and third-order coherence functions  $g^{(n)}(0)$  ( $n=2$  and  $3$ ) of an exciton-polariton condensate are measured and compared to the theory. Contrary to an ideal photon laser, deviation from unity in the second- and third-order coherence functions is observed, thus showing a bunching effect, but not the characteristics of a standard thermal state with  $g^{(n)}(0)=n!$ . The increase in bunching with the order of the coherence function,  $g^{(3)}(0) > g^{(2)}(0) > 1$ , indicates that the polariton condensate is different from a coherent state, a number state, or a thermal state. The measurement of third-order coherence has the advantage, compared to the second-order one, that the difference between a thermal state and a coherent state is more pronounced. The experimental results are in agreement with the theoretical model where polariton-polariton and polariton-phonon interactions are responsible for the loss of temporal coherence.

DOI: [10.1103/PhysRevB.81.033307](https://doi.org/10.1103/PhysRevB.81.033307)

PACS number(s): 71.36.+c, 78.67.De

**I. INTRODUCTION**

In a seminal paper by R. J. Glauber marking the beginning of quantum optics, coherent states were studied as unique states, whose normalized coherence functions  $g^{(n)}(0)$  are unity for all orders  $n$ .<sup>1</sup> It has been shown theoretically and experimentally that a photon laser is well characterized by coherence functions  $g^{(n)}(0)$  close to one at pump intensities well above threshold, thus showing all order coherence, except for a random walk phase diffusion. Bose-Einstein condensation (BEC) of polaritons has recently been the subject of detailed investigations<sup>2,3</sup> and the question of its coherence properties arises. BEC is characterized by a large number of particles sharing the same quantum state. Therefore, it is expected that the state of polariton condensates shows temporal coherence properties leading to a coherence function of coherent state  $g^{(n)}(0)=1$  or  $N$ -particle number state  $g^{(n)}(0)=1-\frac{n-1}{N}$ . However, there are important differences between photon laser and polariton BEC, one of which is that the former is based on stimulated emission of photons from an excited level and population inversion is necessary to reach a threshold, while the latter is based on stimulated cooling of polaritons to the ground state from excited states and BEC threshold condition is given by  $n\lambda_T^2 \approx 2 \ln L/\lambda_T$ , where  $n$ ,  $\lambda_T$ , and  $L$  are the polariton density, thermal de Broglie wavelength, and system size, respectively. Thus, when condensation occurs in a lower polariton (LP) ground state, the population inversion is not created yet in quantum wells.<sup>4,5</sup> Furthermore, scattering processes to the noncondensed polariton modes may influence the coherence properties of the polariton condensate.<sup>6</sup> This last effect is absent in a photon laser. Contrary to a photon laser, deviation from unity in the second-order coherence function  $g^{(2)}(0)$  for the exciton-polariton condensate has been observed<sup>2,7,8</sup> showing a bunching effect. The origin of the deviation from unity has not been well identified so far. However, in recent theoretical papers, the deviation from full coherence in higher order

correlations have been shown.<sup>5,9,10</sup> The model presented in Refs. 5, 9, and 10 considers both polariton-polariton and polariton-phonon scattering. This scattering processes lead to two competing effects that involve the condensed polaritons: resonant scattering into and out of the polariton ground state involving one polariton in the ground state and parametric scattering of two polaritons in the ground state into two states of opposite momentum. Below threshold, the statistics of the polaritons is determined by the thermal phonon bath, which is responsible for polariton relaxation, and the effect of polariton-polariton scattering is negligible. In this case, the corresponding  $g^{(n)}(0)$  is given by that of a thermal state  $n!$ . Above threshold, resonant polariton-polariton and polariton-phonon interactions compete. The parametric scattering between ground state and excited states induces a depletion of the ground-state population. This effect induces fluctuations in the population and manifests itself in a loss of coherence in the polariton condensate.<sup>5,9</sup> Indeed, when higher order coherence functions are calculated, a deviation from full coherence and bunching effect above threshold are obtained.

Let us discuss this point in more detail. The particle statistics of a thermal state are characterized by the geometrical distribution  $p(m)=\frac{1}{\mu+1}\left(\frac{\mu}{\mu+1}\right)^m$ , where  $p(m)$  is a probability of  $m$  polaritons and  $\mu$  is mean polariton number, and lead to a normalized coherence function  $g^{(n)}(0)=n!$ , which grows with  $n$ . In this case, we expect a larger bunching behavior in the higher order coherence functions, such as  $g^{(3)}(0) > g^{(2)}(0)$ . This behavior is indeed found for polaritons in the ground state below threshold.<sup>5</sup> Above threshold, the calculated particle distribution has a shape close to but different from a Poissonian distribution. The second-order coherence function is larger than one and the higher order coherence functions are even larger.<sup>5</sup> In this Brief Report, we present the measurement results of the second and third order normalized coherence functions. In particular, we show that the observed behavior of growing bunching with the order  $n$  agrees well with the theory.

## II. EXPERIMENT

The second-order coherence function for exciton-polariton condensates has been measured for GaAs quantum well (QW) microcavity<sup>2</sup> and CdTe QW microcavity.<sup>7</sup> Below condensation threshold,  $g^{(2)}(0)$  takes almost unity since both polariton emission decay time below threshold and detector response time are much longer than the intensity correlation time of polaritons. Above threshold  $g^{(2)}(0)$  increases steeply and then gradually saturates as the pump intensity goes up. A full coherence  $g^{(2)}(0)=1$  has not been observed even at far above threshold. In the present work, we used 12 GaAs QWs embedded in GaAlAs/AlAs distributed Bragg reflector (DBR) microcavity that was used in our previous experiments.<sup>11,12</sup> The sample has three stacks of four GaAs QWs which are embedded at the central three antinode positions of a DBR planar microcavity. Lateral trapping potential is provided by a hole surrounded by a thin metal (Ti/Au) film which pushes photon-field amplitude antinode position at GaAlAs/air interface inside GaAlAs layer, resulting in the blueshift of the cavity resonance and hence LP energy under the metallic layer. By using this metallic hole structure, we could obtain the confinement of polaritons under a hole, which allows us to access to a single spatial mode in second and third-order coherence measurements. An optical measurement system together with electronics for third order coherence measurement is shown in Fig. 1.

A mode-locked Ti:sa laser with 4 ps pulse width is utilized as a pump laser. It is focused on the sample surface with diameter of about 50  $\mu\text{m}$ . An objective lens collimates the output luminescence and near field image is made at the position of the pinhole by the second lens. Here we can spatially filter the metallic hole area of about 5  $\mu\text{m}$  diameter. Then at the entrance slit of the spectrometer, far field is imaged by the third lens. Dispersion relation can be measured by the spectrometer and an attached nitrogen-cooled charge-coupled device (CCD) camera.

The left-hand side of Fig. 2 is an example of observed dispersion at  $4P_{\text{th}}$  ( $P_{\text{th}}$  is threshold power). In case we use the side exit of the monochromator, the output signal enters Hanbury-Brown Twiss (HBT) setup consisting of two non-polarizing beam splitters and photon detectors. We can measure  $g^{(2)}(0)$  and  $g^{(3)}(0)$  with this setup. Signal entering HBT setup is split into three paths by a 2:1 splitting ratio beam splitter and a 1:1 ratio beam splitter. We used single photon counting modules (Perkin Elmer, SPCM AQR series) for this coherence function measurement. The detectors' response time is relatively slow (about 300 ps timing resolution), but its slow response does not limit our capability of measuring  $g^{(2)}(0)$  and  $g^{(3)}(0)$  since we used a pulsed pump laser of 4 ps pulse width and the emission time becomes shorter than the correlation time at well above threshold. This setup allows us to pick up arbitrary part of condensates at LP ground state by setting appropriate wavelength filter of spectrometer. The in-plane momentum region is determined by collecting optics and actual CCD image size. Area surrounded by dotted line in Fig. 2 is the detected region.

For  $g^{(3)}(0)$  measurement, we need to take threefold coincidence of three detectors. For normalization of coherence function, threefold coincidence rate of simultaneous three

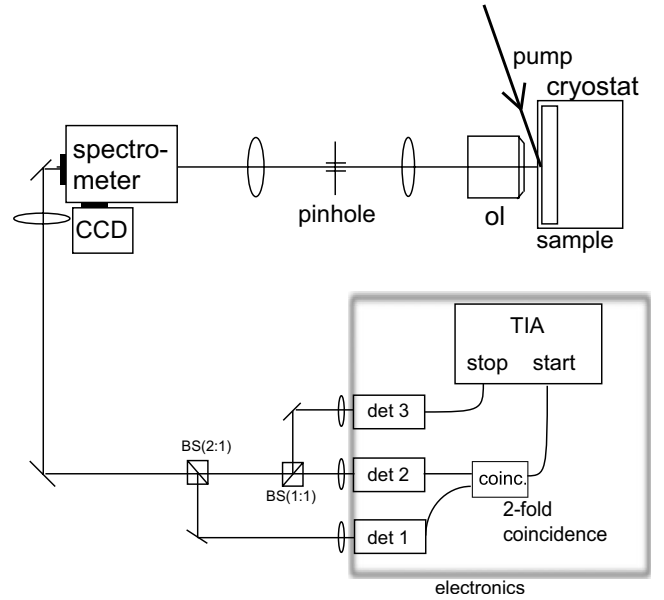


FIG. 1. Experimental setup pump: mode-locked Ti:Sa laser with 76 MHz repetition rate and 4 ps pulse width. GaAs QW microcavity sample is held in a cryostat which keeps the sample temperature at 10 K during experiment. ol is an objective lens with 4 mm focal length and 0.55 NA. Momentum distribution is imaged at the entrance slit of the spectrometer by the ol and the following two lenses. Thus, dispersion curve of LP can be directly observed by the attached CCD camera and LP ground-state emission is spectrally selected. When the signal goes through the other exit, it enters HBT setup. First two beam splitters [BS(2:1) and BS(1:1)] splits the signal into three paths with roughly equal intensities for maximizing threefold coincidence. Electronics consists of electrical processing units for taking twofold or threefold coincidences, i.e., single photon detectors (det 1 to det 3), delay units for timing adjustments, discriminator (delay units and discriminator are not shown in the figure), coincidence unit, and TIA.

photon detection for one pump pulse must be divided by accidental signal (product of independent signal rates of three detectors). In the actual measurement, we used a time interval analyzer (TIA) which measures time difference between start and stop inputs.  $g^{(2)}(0)$  can be directly measured by TIA but  $g^{(3)}(0)$  cannot be since our TIA has just two input channels (start and stop).  $g^{(3)}(0)$  is instead measured by the following method. At first, we took twofold coincidence between detector 1 and detector 2 by twofold coincidence unit. Then the output signal is input to start port of the TIA (Fig. 1). Right-hand side of Fig. 2 is an example of raw histogram taken by TIA. The horizontal axis corresponds to delay time between start signal and stop signal. The interval between next pulses is 13 ns which correspond to repetition period of the pump laser. The highest peak corresponds to threefold coincidence of simultaneously detected three photons for one pump pulse and surrounding peaks correspond to twofold coincidence by simultaneously detected two photons for one pump pulse and accidental third photon from different time slot. So the surrounding peaks correspond to  $g^{(2)}(0)$ , i.e., just detector 1 and detector 2 are fired by the same pulse. In this configuration, we need to preliminary know  $g^{(2)}(0)$  to obtain  $g^{(3)}(0)$  since taking the ratio between central peak and aver-

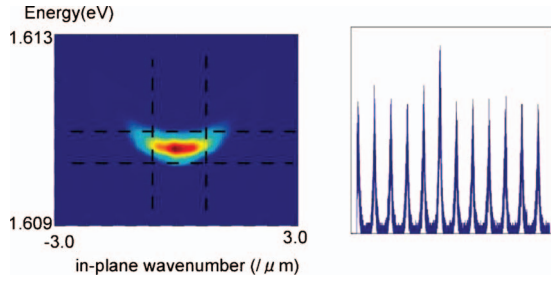


FIG. 2. (Color) (Left) Energy vs wave-number dispersion of LP around  $4P_{th}$ . Closed area surrounded by dotted lines is picked up by using spectrometer and appropriate collection optics. (Right) An example of threefold coincidence TIA data. Note that though it looks the same as usual  $g^{(2)}(0)$  measurement, this histogram is triggered by input signals from twofold coincidence unit, therefore, this histogram gives information of  $g^{(3)}(0)/g^{(2)}(0)$ . The highest peak corresponds to detections of three photons from one pump pulse. Surrounding peaks are twofold coincidence by one pump (start signal of TIA) but the stop signal of TIA is generated by other pump pulses at different time slots. Interval between each peak is 13 ns corresponding to the repetition rate of pump laser.

age of surrounding peaks just gives  $g^{(3)}(0)/g^{(2)}(0)$ . So  $g^{(3)}(0)$  can be obtained by multiplying  $g^{(2)}(0)$  to the ratio of central peak to surrounding peak.

We measured  $g^{(2)}(0)$  and  $g^{(3)}(0)$  at various pump powers (Fig. 3). In Fig. 3, theoretical results are drawn together with experimental data. The details of the theoretical model are given in Ref. 9. Below threshold, though they are not shown in Fig. 3, the statistics obeys thermal distribution, hence, the theory predicts  $g^{(n)}(0)=n!$ . Just above threshold, they begin to gain coherence and rapidly decrease toward unity. However, the decreases stop around  $1.5P_{th}$  due to increasing effect of polariton scattering. As the pump intensity increases, they converge into certain values [ $g^{(3)}(0)\sim 2.5$  and  $g^{(2)}(0)\sim 1.4$ ]. The experimental data shows  $g^{(2)}(0)$  and  $g^{(3)}(0)$  are still close to unity just above threshold. However,

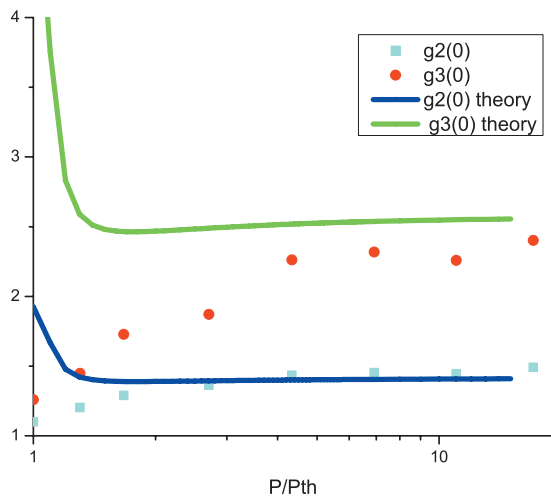


FIG. 3. (Color) Pump intensity dependence of  $g^{(2)}(0)$  and  $g^{(3)}(0)$ .  $P_{th}$  is threshold power. Square:  $g^{(2)}(0)$  and circle:  $g^{(3)}(0)$ . Two curves are calculated coherence functions whose theoretical model is described in Ref. 9.

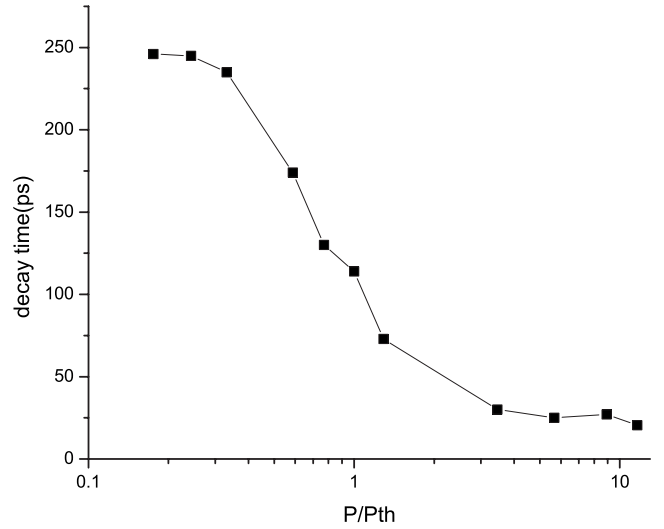


FIG. 4. A photoluminescence decay time of a LP ground state. Around threshold, the decay time gradually decreases. It reaches a minimum value of 20 ps around  $3-4P_{th}$  where  $g^{(2)}(0)$  and  $g^{(3)}(0)$  approach to the theoretical values.

they increase and become closer to theoretical values as the pump intensity increases. After gradual increase, they reach a flat area at around  $4P_{th}$ .

### III. DISCUSSION

To understand the discrepancies between theory and experiment at the pumping regime of  $1 < P/P_{th} < 4$ , we need to consider intensity correlation time and decay time of the condensate emission.

The ground-state photoluminescence decay time measured by a streak camera preceded by a spectrometer is shown in Fig. 4. Since the streak camera was set after a spectrometer, we could avoid the contamination by the non-condensates and the wavelength range giving maximum PL intensities at each pump power was picked up.

Below threshold where photon statistics is expected to obey thermal distribution, the observed statistics is always  $g^{(2)}(0)=g^{(3)}(0)\approx 1$  since decay time  $\tau$  of photoluminescence is much longer than the intensity correlation time  $\Delta\tau_c$ . In the case of longer  $\tau\gg\Delta\tau_c$ ,  $g^{(n)}(\tau)=1$ .<sup>2</sup> The measured  $g^{(n)}(0)$  is the integration of  $g^{(n)}(\tau)$  over an integration time window which is given by an emission time  $\tau$  in our case basically given by Fig. 4, hence, it is close to unity after averaged over the whole emission lifetime. Just above threshold, the condition is still the same because the emission pulse width is longer than the intensity correlation time until the pump rate becomes  $4P_{th}$  where, as indicated in Fig. 4, the decay time reaches its shortest value of about 20 ps. From that point far above threshold, the intensity correlation time becomes closer to the emission decay time, and then the intrinsic noise property of the condensates begins to be detected properly.

In case of pulsed excitation, the energy of the condensate shifts during the decay dynamics<sup>13</sup> because the polariton number in ground state and the exciton number in reservoir change in time. The usage of a single mode cw laser as a

pump source helps to get a stationary excitation density and the experimental results may compare better with the theoretical calculations. However, disadvantage of a cw laser pump is that the observed coherence function is affected by the slow time resolution of the detection electronics<sup>7</sup> which is about 300 ps determined by the timing jitter of the single photon detectors. With a cw laser, the signal within the time resolution of the detection electronics is considered to be simultaneous even if it is outside of correlation time of condensate photoluminescence and the observed coherence functions become smaller than their true values again due to the averaging effect as indicated above. On the other hand, exciting the sample with a strong laser pulse and looking at its relaxation dynamics, which develops in a time much shorter than the repetition rate of a mode-locked laser, can avoid these spurious effects.

#### IV. CONCLUSIONS

In conclusion, we have experimentally measured the second- and third-order coherence functions. The observed bunching effect is the experimental evidence for the relatively strong thermal and quantum depletion of the LP condensate. This higher order coherence function measurement technique may contribute to a further investigation of coherence property of an exciton-polariton condensate.

#### ACKNOWLEDGMENTS

T.H. thanks G. Roumpos, N. Y. Kim, and S. Utsunomiya for their help. T.H. and Y.Y. acknowledge financial support from NICT, Special Coordination Funds for Promoting Science and Technology, MEXT, and DARPA.

<sup>1</sup>R. J. Glauber, *Phys. Rev.* **130**, 2529 (1963).

<sup>2</sup>H. Deng, G. Weihs, C. Santori, J. Bloch, and Y. Yamamoto, *Science* **298**, 199 (2002).

<sup>3</sup>J. Kasprzak, M. Richard, S. Kundermann, P. Jeambrun, J. M. J. Keeling, F. M. Marchetti, M. H. Szymańska, R. André, J. L. Staehli, V. Savona, P. B. Littlewood, B. Deveaud, and Le Si Dang, *Nature (London)* **443**, 409 (2006).

<sup>4</sup>A. Imamoğlu, R. J. Ram, S. Pau, and Y. Yamamoto, *Phys. Rev. A* **53**, 4250 (1996).

<sup>5</sup>P. Schwendimann and A. Quattropani, *Phys. Rev. B* **77**, 085317 (2008).

<sup>6</sup>D. Porras and C. Tejedor, *Phys. Rev. B* **67**, 161310(R) (2003).

<sup>7</sup>J. Kasprzak, M. Richard, A. Baas, B. Deveaud, R. André, J.-Ph. Poizat, and Le Si Dang, *Phys. Rev. Lett.* **100**, 067402 (2008).

<sup>8</sup>A. P. D. Love, D. N. Krizhanovskii, D. M. Whittaker, R.

Bouchekioua, D. Sanvitto, S. A. Rizeiqi, R. Bradley, M. S. Skolnick, P. R. Eastham, R. André, and L. S. Dang, *Phys. Rev. Lett.* **101**, 067404 (2008).

<sup>9</sup>D. Sarchi, P. Schwendimann, and A. Quattropani, *Phys. Rev. B* **78**, 073404 (2008).

<sup>10</sup>T. D. Doan, H. T. Cao, D. B. Tran Thoai, and H. Haug, *Phys. Rev. B* **78**, 205306 (2008).

<sup>11</sup>C. W. Lai, N. Y. Kim, G. Roumpos, H. Deng, M. D. Fraser, T. Byrnes, P. Rechter, N. Kumada, T. Fujisawa, and Y. Yamamoto, *Nature (London)* **450**, 529 (2007).

<sup>12</sup>S. Utsunomiya, L. Tian, G. Roumpos, C. W. Lai, N. Kumada, T. Fujisawa, M. Kuwata-Gonokami, A. Löffler, S. Höfling, A. Forchel, and Y. Yamamoto, *Nat. Phys.* **4**, 700 (2008).

<sup>13</sup>D. Sanvitto, A. Amo, L. Viña, R. André, D. Solnyshkov, and G. Malpuech, *Phys. Rev. B* **80**, 045301 (2009).